J. Fluid Mech. (2001), *vol.* 446, *pp.* 67–93.
DOI: 10.1017/S0022112001005596 Printed in the United Kingdom

Saturated Rayleigh–Taylor instability of an oscillating Couette film flow

By DAVID HALPERN AND ALEXANDER L. FRENKEL

Department of Mathematics, University of Alabama, Tuscaloosa, AL 35487, USA

(Received 24 March 1999 and in revised form 10 May 2001)

The nonlinear stability of a two-fluid system consisting of a viscous film bounded above by a heavier and thicker layer, between two horizontal plates, with one of the plates oscillating horizontally about a fixed position, is investigated. An evolution equation governing the thickness of the viscous film is derived. Numerical simulations of this equation on extended spatial intervals demonstrate nonlinear small-amplitude saturation of the Rayleigh–Taylor instability in certain parametric regimes. In the low-frequency time-asymptotic regimes, the averaged properties of the extensive spatio-temporal chaos are not steady, but rather oscillate in time. A quasi-equilibrium theory is proposed in which the low-frequency results are interpreted by building upon the notions developed earlier for the simpler case of a non-oscillatory film governed by the classical, constant-coefficient Kuramoto–Sivashinsky equation. In contrast, the higher-frequency solutions exhibit piecewise linear profiles that have never been encountered in simulations of non-oscillatory films. The amplitude as a function of frequency has a single minimum point which is of order one. Also, preliminary results of numerical simulations of film evolution are given for the large-amplitude parametric regimes. At some parameter values, rupture is observed, similar to the case with no base flow; in other regimes the basic flows succeeds in preventing rupture. The complete characterization of the factors responsible for the particular asymptotic fate of the film, rupture or no rupture, remains an open question.

1. Introduction

It is well recognized that the gravitational, 'Rayleigh–Taylor', instability (Rayleigh 1883; Taylor 1950) of fluid layers occurs in a variety of engineering and physical situations, ranging from coating flows with paint or photographic material, to the boiling of liquids (Berenson 1962), to inertial confinement fusion experiments in which pellets of deuterium–tritium fuel undergo laser implosion (Kilkenny *et al.* 1994; Berning & Rubenchik 1998), to certain geophysical processes (Whitehead 1988; Canright & Morris 1993; Ribe 1998). In many applications, rupture, such as in the break up of the shell containing the fuel before the fuel is fully compressed in inertial confinement fusion, is an undesirable event.

The linear theory of the Rayleigh–Taylor instability is documented in Chandrasekhar (1961), and later developments, including the work on two-layer Couette flows of fluids with different densities, are discussed in the book of Joseph & Renardy (1991). The instability is a long-wave one, the short waves being damped by surface tension. Within the last twenty years, significant advances have been made in understanding the nonlinear development of the longwave regime of the Rayleigh–Taylor

instability of a viscous film. The case of a steady linear basic velocity profile between two plates (plane two-fluid Couette flow) has been investigated by Babchin *et al.* (1983), who derived an evolution equation of the Kuramoto–Sivashinsky (KS) type for the undulation of the interface between the two fluids using a weakly nonlinear analysis. They showed that, for a range of the basic velocity shear rate, film rupture is prevented owing to the nonlinear saturation of the instability such that the amplitude of the interfacial waves remains small as compared to the average film thickness. Yiantsios & Higgins (1989) examined the two-dimensional Rayleigh–Taylor instability of a two-fluid system with no basic velocity field. They found numerically that if gravitational effects are sufficiently weak, so that the Bond number is smaller than some critical value, formation of stable pendant drops is possible, with a much thinner film of fluid spanning the space between the drops. Above this critical value, drop break-up occurs. Fermigier *et al.* (1992) considered three-dimensional instabilities of the same system and the dynamics of pattern selection. They found experimentally that at large times, drop coalescence is possible leading to drop break-up and dripping even at small Bond numbers. Also, a three-dimensional Rayleigh–Taylor instability was examined numerically by Tryggvason & Unverdi (1990).

The effect of an oscillatory primary flow on single-fluid systems has been shown to be either linearly stabilizing or destabilizing (Hall 1975; Davis 1976; von Kerczek 1982, 1987). Or (1998) has extended the pioneering work of Yih (1968) in the instability of a fluid layer supported by a horizontal plate oscillating in its own plane by including disturbances whose wavelength is not large. For two-fluid oscillatory Couette flows between two horizontal plates, the two-dimensional linear stability was considered by Coward & Papageorgiou (1994). In the case they studied, the densities are equal, and one of the plates moves with a velocity that consists of a steady part, as in Babchin *et al.* (1983), combined with a smaller oscillatory term. They concluded that the interface between the two layers is unstable if the thinner of the two layers contains the more viscous fluid as in the case of steady Couette flow (Yih 1967). Coward & Papageorgiou (1994) found that the effect of oscillations can be either stabilizing or destabilizing depending on parameters. King, Leighton & McCready (1999) studied the same system and confirmed experimentally their linear-theoretical results. They showed that the results can be derived by combining those for the purely oscillatory and purely steady flows. Coward & Renardy (1997) extended the results of Coward & Papageorgiou (1994) by considering the effects of arbitrary wavelength and adding a streamwise pressure gradient consisting of a steady part and an oscillatory component, which may have a phase shift with respect to the oscillating top plate. Halpern, Moriarty & Grotberg (1999) considered the effects of a periodic shear stress on the linear stability of a thin film coating the inner surface of a compliant tube, to simulate the effects of oscillatory airflow on pulmonary airway closure. This system is an example of a core–annular flow, which has certain similarities to the Rayleigh–Taylor system. Examples of non-oscillatory core–annular flows include separated flow of steam and water in power generation facilities, lubricated pipelining of crude viscous oils (see Joseph & Renardy 1991), and air flow through the small airways of the lungs which are coated with a thin viscous film (Johnson *et al.* 1991; Halpern & Grotberg 1992). In the core–annular film flow, the destabilizing factor is the component of capillary forces due to the azimuthal curvature of the interface, which may cause the fluid core to break up.

In the first weakly nonlinear theory for a steady core–annular flow, Frenkel *et al.* (1987) have shown that there are parametric regimes such that the growth of the inter-

face undulation is arrested by nonlinear effects described by a Kuramoto–Sivashinsky equation. The subsequent work on nonlinear regimes of core–annular flows included the papers by Frenkel (1988); Papageorgiou *et al.* (1990); Frenkel & Kerchman (1994); Kerchman (1995). In Frenkel (1988) and Papageorgiou *et al.* (1990) a modified Kuramoto–Sivashinky equation was derived which included the dispersive effect of viscosity stratification between the core and the annular film. This dispersive effect was shown to produce less chaotic flows. The weakly nonlinear instability of an oscillatory core–annular flow was considered by Coward, Papageorgiou & Smyrlis (1995) for the case where the pressure gradient driving the core flow is a constant modified by a smaller oscillatory term (which therefore can be called the 'weakly oscillatory' case). They obtained a Kuramoto–Sivashinsky equation (also including the dispersive terms due to sufficiently large viscosity contrast) with time-periodic coefficients having a non-zero mean, and simulated this equation for a range of spatial intervals. They documented extensive computations and characterizations of routes to chaos and quasi-periodic regimes. As far as we know, the nonlinear development of the Rayleigh–Taylor instability (or, for that matter, any other instability of a *two-layer Couette* flow) for the oscillatory case has not been studied before.

In this paper, we investigate the Rayleigh–Taylor instability of a two-fluid system between two horizontal plates, with the bottom plate fixed and the top plate oscillating in its plane with a zero-mean velocity. The bottom fluid is a viscous film bounded below by the fixed plate and above by a thicker layer of a denser liquid. The case with zero-mean velocity can be expected to be significantly different from that of a flow where the direction of the velocity is never reversed. This is because the basic flow is responsible for arresting the growth of interfacial waves (Babchin *et al.* 1983), but this mechanism is not effective when the basic velocity is close to zero. It is known that in the case of no primary flow the film ruptures, and the rupture time can be estimated from the linear theory, the nonlinear theory giving some quantitative corrections, but not making any qualitative difference and still predicting rupture. With the steady Couette flow, the linear stability theory still predicts instability suggesting breakup, but the nonlinear theory leads to the qualitatively different conclusion, the small-amplitude saturation of instability and thus prevention of rupture. The zero-mean oscillatory primary flow combines the periods of almost zero flow with those of almost steady flow. These point in the opposite directions as to the breakup of the film. Therefore, the principal question arises whether the small-amplitude saturation of instability, keeping the film from breakup, is still possible. This issue was our motivation for undertaking the present work. Also, as was mentioned above, the nonlinear stability of oscillatory flows is important in pulmonary airway closure.

In § 2, the basic oscillatory flow for the uniform-thickness case is determined. This flow is Rayleigh–Taylor unstable to long-wave disturbances as was mentioned above. The nonlinear evolution of disturbances is considered in § 3. Using a weakly nonlinear multiparameter analysis, a modified Kuramoto–Sivashinsky equation for the interface deviation is obtained, together with the parametric constraints appropriate for the low-frequency regimes, and with a quasi-equilibrium theory predicting the form of the solutions. The behaviour of this equation is studied numerically over large spatial domains, assuming periodic boundary conditions. Low-frequency numerical results are presented in § 4, and comparisons are made with the canonical KS solutions, and with the predictions of the quasi-equilibrium theory of § 3. Some preliminary results for high frequencies are given in § 5, and for large-amplitude regimes in § 6. Finally, § 7 gives a concluding discussion of the results.

2. Basic flow

Consider a two-fluid system between two horizontal plates, a distance $h+H$ apart, with the top plate oscillating sinusoidally at a frequency Ω and the bottom plate fixed. A thin film of constant viscosity μ, and density ρ_F, is bounded below by the fixed plate at $y=-h$, and above ($y=0$) by a fluid layer (of thickness H) that has a higher density $\rho_L > \rho_F$. For simplicity, we assume that the two fluids have the same viscosity, μ. For the basic unidirectional (horizontal) flow, when the interface between the two fluids is flat, the only non-trivial Navier–Stokes (NS) equations, the x-momentum equations, reduce to one-dimensional diffusion equations:

$$\rho_j U_{j_t} = \mu U_{j_{yy}}, \tag{2.1}$$

where U_j is the horizontal fluid velocity, $j=F$ for the film and $j=L$ for the top liquid. In addition to the no-slip conditions at the plates (in particular, $U_L(H,t) \propto \sin(\Omega t+\phi)$, $-\infty < t < \infty$, where ϕ is a constant phase), there are those of continuity of both velocity and shear stress at the interface $y=0$: $U_F(0,t) = U_L(0,t)$, $U_{Fy}(0,t) = U_{Ly}(0,t)$. The (flat-interface, Nusselt-type) solution to this problem can be written, without loss of generality, as

$$U_j(y,t) = U_0 \mathrm{Re}\left(\mathrm{e}^{\mathrm{i}\Omega t}\left(\frac{\sinh k_j y}{k_j h} + \frac{\cosh k_j y}{Ch}\right)\right), \tag{2.2}$$

(where Re designates the real part, $k_j := (\rho_j \Omega/\mu)^{1/2}\mathrm{e}^{\mathrm{i}\pi/4}$, and $C := k_F \coth k_F h$; here and below we use $:=$ to indicate the definition of a quantity), so that the velocity shear rate at the interface has the convenient form $(\partial U_j/\partial y)(0,t) = W_0 \cos \Omega t$. Here,

$$W_0 := U_0/h. \tag{2.3}$$

It is convenient for what follows to treat W_0, and not the top plate velocity amplitude, as the independent parameter of oscillations. The convenient phase for interfacial shear-rate oscillations can be achieved, of course, by an appropriate choice of the time origin.

The hydrostatic pressure and velocity profile (2.2), the same as the pressure in the stagnant-film case, comprise the base flow solution satisfying all the differential equations and boundary conditions of the NS problem.

For small enough Ω, U_j is nearly linear in y at each time. This is shown in figure 1, where U is plotted versus y at three instances of time, for $\Omega = 1/300$ and for the indicated values of the other parameters. Below, we will assume that, by default, Ω is small enough, so that the lengthscales $1/|k_j|$ of the base flow are large, $|k_j|h \ll 1$.

3. Weakly nonlinear equation for the evolution of disturbances

Considering the evolution of a one-dimensional disturbance of the basic oscillatory flow, we start with the hypothesis, in line with our principal motivation of comparing with the non-oscillatory case of Babchin *et al.* (1983), that there is still a range of parameters within which the exact NS problem (see Appendix) can be reduced, by discarding a number of terms in the equations, to the simplified form which was used, to a good approximation, in the simpler cases of Babchin *et al.* (1983) and Yiantsios & Higgins (1989). The bulk momentum and incompressibility equations of the simplified disturbance problem for the film describe a Stokes flow in the

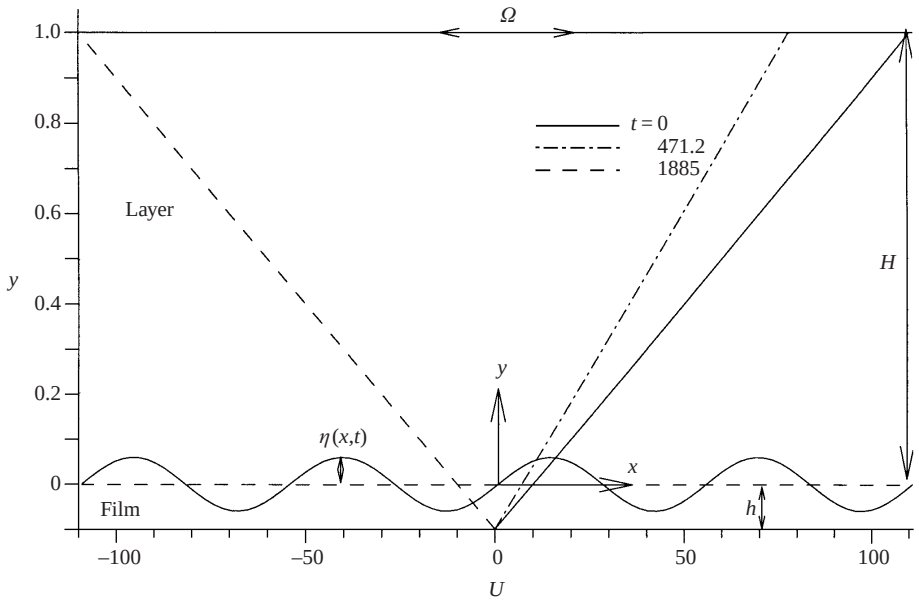

FIGURE 1. The oscillating basic velocity profile, U, at small frequency, $\Omega = \frac{1}{300}$, is essentially linear at all times as represented by the three instances shown. $\rho_F = 0.9$; $\rho_L = 1$; $\mu = 1$; $W_0 = 100$; $\Omega = \frac{1}{300}$ (CGS units).

lubrication approximation:

$$u_{yy} = \frac{1}{\mu}\, p_x, \tag{3.1}$$

$$p_y = 0, \tag{3.2}$$

$$v_y = -u_x, \tag{3.3}$$

where $u(x, y, t)$ and $v(x, y, t)$ are the disturbances of the horizontal and vertical components of the velocity disturbance and $p(x, y, t)$ is the disturbance of the pressure field. At the fixed bottom plate, the no-slip boundary condition is

$$u(y = -h) = v(y = -h) = 0, \tag{3.4}$$

and at the liquid–liquid interface – assuming, in particular, that the disturbances of the top fluid are, as in the earlier papers, negligible – the balances of the normal and tangential stresses give

$$p(y = \eta) = -\sigma\eta_{xx} - g(\rho_L - \rho_F)\eta := \Pi\,(x, t), \tag{3.5}$$

$$u_y(y = \eta) = mU_{Ly}(y = \eta) - U_{Fy}(y = \eta) := S(x, t), \tag{3.6}$$

where $\eta(x, t)$ determines the interface, $y = \eta(x, t)$, $m = \mu_L/\mu_F$ is the viscosity ratio, σ is the interfacial tension, and g is the acceleration due to gravity. (For the moment, to derive a more general evolution equation, we allow for the viscosities to be different.) This simplified description, having the merit of yielding a single evolution for $\eta(x, t)$, presupposes a number of parametric conditions. In particular, the lengthscale (in general, changing with time) λ of the disturbances is assumed here to be long compared with the depth of the film, h, so that $h/\lambda \ll 1$. In order to drop the

time derivative and advective terms from the Navier–Stokes equations, we require that the Reynolds number and the ratio of the time-dependent to viscous terms be small, i.e. $(U_0 h/\nu_F)h/\lambda \ll 1$ and $h^2/(\nu_F \Upsilon) \ll 1$, where Υ is the characteristic timescale and ν_j is the kinematic viscosity, $\nu_j = \mu/\rho_j$. Neglecting the disturbances of the top fluid requires that their vertical lengthscale be large, $|k_L|h \ll 1$. In § 3.2, after the dissipative evolution equation is obtained and yields the characteristic scales of all the variables, we find the complete set of such parameter constraints. They follow from the consistency requirement that the terms of the NS equations (see Appendix) which have been discarded in the transition to the simplified problem be much smaller than the terms retained, i.e. those appearing in (3.1)–(3.6). We show that there is a non-empty range of parameters where all the constraints are satisfied, and our single-equation description of evolution should be a good approximation. Since the constraints require that a number of dimensionless groups be independently small, this technique of the derivation of evolution equations has been termed 'the multiparameter perturbation approach' (see, e.g. Frenkel *et al.* (1987); for a discussion of this method, see Frenkel & Indireshkumar 1996, 1999).

The velocity and pressure disturbances in the film, given by

$$u(x,\tilde{y},t) = S\tilde{y} + \frac{\Pi_x}{\mu}\left(\tfrac{1}{2}\tilde{y}^2 - \tilde{y}\tilde{h}\right), \tag{3.7}$$

$$v(x,\tilde{y},t) = -\frac{\Pi_{xx}}{\mu}\frac{\tilde{y}^3}{6} + \left(\frac{\Pi_x \tilde{h}}{\mu} - S\right)_x \tfrac{1}{2}\tilde{y}^2, \tag{3.8}$$

$$p(x,\tilde{y},t) = \Pi(x,t), \tag{3.9}$$

where $\tilde{y} = y + h$, can be readily verified to be the solution of (3.1)–(3.6). Substituting these expressions into the kinematic boundary condition

$$\eta_t + U_F(\eta,t)\eta_x + u(\eta,t)\eta_x = v(\eta,t), \tag{3.10}$$

yields the evolution equation

$$\tilde{h}_t + D\tilde{h}_x + \frac{1}{3\mu_F}(\tilde{h}^3(\delta\tilde{h} + \sigma\tilde{h}_{xx})_x)_x = 0, \tag{3.11}$$

where $\tilde{h} = h + \eta$, $\delta = g(\rho_L - \rho_F)$, and

$$D = \left\{U_F + [mU_{Ly} - U_{Fy}]\tilde{h} + [mU_{Lyy} - U_{Fyy}]\tfrac{1}{2}\tilde{h}^2\right\}_{y=\eta}. \tag{3.12}$$

Equations (3.11) and (3.12) have been obtained here without specifying the basic velocity profiles $U_j(y,t)$. So they can be used for different film systems, with the appropriate changes in (3.11) accounting for different stabilizing and destabilizing factors. For example, for a core–annular configuration, the destabilizing effect comes from the transverse component of interfacial curvature, and therefore δ is replaced by σ/a^2, where a is the radius of the core.

A further simplification to (3.11) ensues if it is assumed that (i) the characteristic lengthscale of the basic flow is large (which is always the case in the low-frequency limit $\Omega \to 0$),

$$|k_F|h \ll 1, \tag{3.13}$$

(we also assume $\rho_F \sim \rho_L \sim \rho$, say) and (ii) the disturbance remains small-amplitude,

$$\eta \ll h. \tag{3.14}$$

By making a coordinate transformation $\tilde{x} = x - \int^t U_j(0,\tau)\,\mathrm{d}\tau$, corresponding to a reference frame of the basic interface, and using the leading terms of the Taylor series about $\eta = 0$ in (3.11) and (3.12), we obtain the following equation for η:

$$\eta_t + W_0 \cos \Omega t \; \eta \; \eta_x + \frac{h^3}{3\mu}(\delta \eta_{xx} + \sigma \eta_{xxxx}) = 0, \tag{3.15}$$

where the tilde has been dropped. Here, the nonlinear term is due to the first term of (3.12); the contributions of all the other terms of (3.12) are much smaller owing to the constraint (3.13). We note that essentially the same evolution equation would be obtained for the case when the top plate is fixed and the bottom one oscillates, or when both plates oscillate with the same frequency. This is the case because we can always shift to the reference frame in which the bottom plate is at rest. The Navier–Stokes equations in this non-inertial frame would include terms equivalent to oscillatory, horizontal components of the acceleration due to gravity, but those drop out in the transition to the problem of disturbances. Also, the basic velocity changes only by a term which depends only on time, so its y-derivative which appears in the equations for disturbances remains the same. Thus the equations and boundary conditions of the disturbances are essentially unchanged, and lead to the same evolution equation (3.15).

Equation (3.15) can be rescaled into a standard form by letting $\bar{x} = x/\Lambda$, $\eta = A\bar{\eta}$, $\bar{t} = t/T$ and $\bar{\Omega} = \Omega T$, where

$$\Lambda = \left(\frac{\sigma}{\delta}\right)^{1/2}, \qquad T = \frac{3\mu\sigma}{h^3\delta^2}, \qquad A = \frac{h^4\delta^{3/2}}{3\mu U_0 \sigma^{1/2}}. \tag{3.16}$$

(Λ, T and A are the time-asymptotic characteristic amplitude, lengthscale and timescale, respectively, which render all the terms of the evolution equation to be pairwise balanced when the nonlinear coefficient is near its maximum value, $\cos \Omega t \sim 1$). As a result, we arrive at the dimensionless evolution equation

$$\eta_t + \cos \Omega t \; \eta \; \eta_x + \eta_{xx} + \eta_{xxxx} = 0, \tag{3.17}$$

(where the bars over all the variables and the constant Ω have been dropped). This equation is clearly of the Kuramoto–Sivashinsky type, but the nonlinear term has an oscillatory factor. (A similar equation has been derived by Coward *et al.* (1995) (for a different, core–annular system), but with the coefficient of the nonlinear term in (3.17) consisting of a bigger constant part and a smaller oscillatory term, in contrast to the 'strongly oscillatory', i.e. zero on average, case of (3.17).)

Equation (3.17) has the same linear stability characteristics as the canonical, constant-coefficient, KS equation. A normal-mode analysis is carried out by letting $\eta \propto \mathrm{e}^{\gamma t + \mathrm{i}kx}$, where γ is the growth rate of an infinitesimal disturbance, and k its wavenumber. Substituting this expression into (3.17) yields the dispersion relation

$$\gamma = k^2 - k^4. \tag{3.18}$$

Disturbances grow with time if $0 < k < 1$, with a maximum γ_m of γ being $\gamma_m = \frac{1}{4}$ at $k = 2^{1/2}$, but decay for $k > 1$ owing to the stabilizing effect of the surface tension on the short-wave disturbances.

The constants Λ and T of (3.16) are, respectively, the characteristic lengthscale and timescale of the disturbance evolution on its both linear and the time-asymptotic, (weakly) nonlinear stages. The asymptotic amplitude A is connected to them by the order-of-magnitude relation $A/h \sim (\Lambda/T)/U_0$.

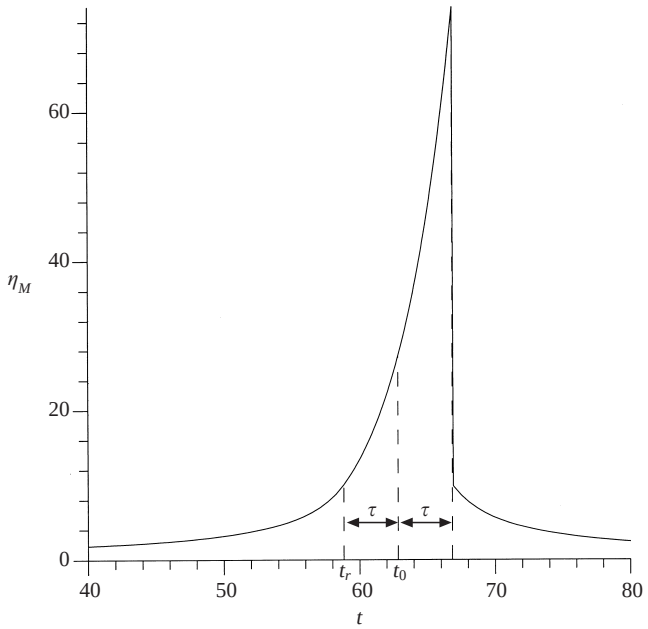

FIGURE 2. Time dependence of the amplitude η_M of the interface deflection given by the quasi-equilibrium model equation (3.20), for $\Omega = 0.025$; $t_0 = 62.83$ and $\tau = 4$.

3.1. *Quasi-equilibrium approximation*

If the coefficient of the nonlinear term in (3.17) had a constant value, K, it is known (Babchin *et al.* 1983) that there would be a pairwise balance of terms in the time-asymptotic regime, which leads to the estimate of the amplitude $\eta \sim K^{-1}$. Suppose now that the value of the constant instantaneously jumps from K to K_1 and remains equal to K_1 afterwards. Then the amplitude will change from the initial K^{-1} to the terminal K_1^{-1} value over a time of the order γ_m^{-1}. It is then reasonable that when the coefficient varies continuously as in (3.17), the amplitude will have the corresponding 'quasi-equilibrium' value $\eta_E(t)$ given by

$$\eta_E \sim \frac{1}{|\cos \Omega t|}, \tag{3.19}$$

as long as the instantaneous rate of change γ_i of the coefficient, $\gamma_i := (\mathrm{d}/\mathrm{d}t)/(\log \eta_E)$, is much smaller than the 'relaxation rate' $\gamma_m = \frac{1}{4}$. Clearly, $\eta_E \to \infty$ as $t \to t_0$, and also $\gamma_i \to \infty$, where t_0 is defined by $\cos \Omega t_0 = 0$; hence $\Omega t_0 = \frac{1}{2}\pi$. We can assume that the amplitude has its quasi-equilibrium value η_E almost all the way, except for a short period of time of length 2τ about the time t_0 during which γ_i is not sufficiently small, viz. $\gamma_i \geqslant \gamma_m$. Also, during this short time interval the nonlinear term is almost zero, so we can assume that the amplitude grows exponentially, as if governed by the linear theory. Thus, the model amplitude η_M (see figure 2) is given by

$$\eta_M(t) \sim \begin{cases} \eta_E(t) = \dfrac{1}{|\cos \Omega t|} & \text{for } t < t_r \text{ or } t > t \geqslant t_r + 2\tau, \\ \eta_E(t_r) \exp(\gamma_m(t - t_r)) = \dfrac{1}{|\cos \Omega t_r|} \exp\,(\gamma_m(t - t_r)) & \text{for } t_r < t < t_r + 2\tau, \end{cases} \tag{3.20}$$

where t_r is defined by $\gamma_i(t_r) = \gamma_m$. Here,

$$\gamma_i(t_r) = \frac{\mathrm{d}}{\mathrm{d}t} \log \frac{1}{|\cos \Omega t_r|} = \Omega \frac{\sin \Omega t_r}{\cos \Omega t_r} = \Omega \frac{\sin(\Omega t_0 - \Omega \tau)}{\cos(\Omega t_0 - \Omega \tau)}. \tag{3.21}$$

Since $\Omega t_0 = \frac{1}{2}\pi$ and $\tau \sim 1$ with $\Omega \ll 1$, so that $\Omega\tau \ll 1$, the last expression simplifies as follows:

$$\Omega \frac{\sin(\frac{1}{2}\pi - \Omega\tau)}{\cos(\frac{1}{2}\pi - \Omega\tau)} \approx \Omega \frac{\sin \frac{1}{2}\pi}{\sin \Omega\tau} \approx \frac{1}{\tau}. \tag{3.22}$$

Thus $\gamma_i(t_r) \approx \tau^{-1}$, and since it should be equal to $\gamma_m = \frac{1}{4}$, it follows that $\tau = 4$, justifying the assumption $\tau \sim 1$ above. Clearly, these considerations are rather crude, and therefore can be expected to predict the scaling of the maximum amplitude with the frequency correctly, but not the constant coefficient of that dependence. It is reasonable to expect that the real value of the maximum amplitude, $\eta_{max} := \max_t \eta_m(t)$ (where $\eta_m(t) := \max_x \eta(x,t)$), lies between $\eta_M(t_r)$ and $\eta_M(t_r + 2\tau)$, that is

$$\tfrac{1}{4}\Omega^{-1} \leqslant \eta_{max}(\Omega^{-1}) \leqslant \tfrac{1}{4}\Omega^{-1} \exp(\gamma_m 2\tau) = \tfrac{1}{4}\Omega^{-1} \exp(2) \tag{3.23}$$

Numerical experiments confirm the Ω^{-1} scaling of the amplitude (see figure 6).

3.2. *Parameter constraints*

In deriving the evolution equation (3.17) using the multiparameter perturbation approach, we have dropped a number of terms from the exact equations of the problem. For consistency, these terms must be much smaller than the terms that are retained. This requirement entails certain constraints on the parameters of the system. Those parameter constraints are considered below.

We can estimate all the terms of the exact problem in the time asymptotic regime since the characteristic scales of the solution are known. Namely, the characteristic lengthscale of film disturbances in the vertical direction is the average film thickness h so that, for the purpose of estimates $\partial/\partial y \sim 1/h$, $\partial^2/\partial y^2 \sim 1/h^2$, etc. The horizontal, x-derivatives are estimated similarly by using the fact that the characteristic lengthscale in the x-direction is given by $\Lambda = (\sigma/\delta)^{1/2}$, and the time-derivatives are estimated with the timescale $T = 3\mu\sigma/h^3\delta^2$ (3.16). Neglecting the x-derivative as compared to the y-derivative of the velocities in the viscous terms implies $\Lambda \gg h$, that is the parameter constraint

$$B^{1/2} = \frac{h\delta^{1/2}}{\sigma^{1/2}} \ll 1 \tag{3.24}$$

(where, recalling the definition, $\delta = g(\rho_L - \rho_F)$, and $B := h^2\delta/\sigma$ is the Bond number, which is thus small). To estimate other terms, we require the estimate of the maximum equilibrium amplitude, $\eta_{\max}$, which follows from the quasi-equilibrium approximation. In order for this approximation to be good, we must require $\Omega \ll 1$, or since $\Omega = \Omega^* T$, where Ω^* is the dimensional frequency,

$$\Omega^* \ll \frac{h^3\delta^2}{\mu\sigma}. \tag{3.25}$$

On the other hand, the frequency of the top plate is required to be sufficiently large to prevent excessive growth of the disturbance due to the destabilizing terms in (3.17), so that η remains small as compared to h. The latter requirement means that $\eta_{max} \ll h/A$, where $A = h^4\delta^{3/2}/3\mu U_0\sigma^{1/2}$ (see equation (3.16)). From (3.23), $\eta_{max} \sim 1/\Omega$. Thus, we obtain the parameter constraint $1/\Omega \ll h/A$, or in terms of the original dimensional

parameters, $h^6\delta^{7/2}/\Omega^*\mu^2\sigma^{3/2}U_0 \ll 1$. This inequality can also be written in the form separating the parameters of motion, U_0 and Ω^*, from the fluid parameters:

$$\Omega^* U_0 \gg \frac{h^6\delta^{7/2}}{\mu^2\sigma^{3/2}}. \tag{3.26}$$

The condition $|kh| \ll 1$ becomes the following constraint in terms of the original dimensional parameters: $(\Omega^{*1/2}/v^{1/2})h \ll 1$, or

$$\Omega^* \ll \frac{\mu}{\rho h^2}. \tag{3.27}$$

The advective terms in the Navier–Stokes are negligible if $U_0 h^2/\Lambda v_F \ll 1$, or

$$U_0 \ll \frac{\sigma^{1/2}\mu}{h^2\delta^{1/2}\rho}. \tag{3.28}$$

Then, the requirement that the time-derivative terms are small is satisfied as a consequence of (3.25), (3.26) and (3.28), and so it does not lead to additional constraints.

Combining (3.26) and (3.28) yields

$$\Omega^* \gg \frac{\rho h^8\delta^4}{\mu^3\sigma^{7/2}}. \tag{3.29}$$

Thus Ω^* is bounded away from zero by a quantity independent of U_0.

Requiring that the viscous terms in the y-momentum equation (3.2) be negligible, and using the expressions (3.8) and (3.9) for v and p in terms of Π and S defined by equations (3.5) and (3.6) with the Taylor expansion $S = ([mU_{Lyy} - U_{Fyy}]_{y=0})\eta$, we obtain the parameter constraint $U_0\Omega^* h/\Lambda g \ll 1$, or

$$U_0\Omega^* \ll \frac{\sigma^{1/2}g}{\delta^{1/2}h}. \tag{3.30}$$

(Then, the S terms in (3.7)–(3.8) are negligible.) All the independent constraints on U_0 and Ω^* above can be summarized as follows:

$$U_0 \ll \frac{\sigma^{1/2}\mu}{h^2\delta^{1/2}\rho}, \quad \Omega^* \ll \min\left(\frac{h^3\delta^2}{\mu\sigma}, \frac{\mu}{\rho h^2}\right), \quad \frac{h^6\delta^{7/2}}{\mu^2\sigma^{3/2}} \ll \Omega^* U_0 \ll \frac{\sigma^{1/2}g}{\delta^{1/2}h}. \tag{3.31}$$

The only other independent constraint is (3.24) which does not involve either U_0 or Ω^*. Other such constraints which are not independent but follow from (3.31) are

$$\frac{h^5\delta^2\rho}{\sigma\mu^2} \ll 1, \quad \frac{h^7\delta^4}{\mu^2\sigma^2 g} \ll 1. \tag{3.32}$$

In the above estimates, $\rho_L \sim \rho_F \sim \rho$, etc.

In a more formal version of this multiparameter technique, the evolution equation is obtained by using multiparameter expansions in powers of several independently small parameters corresponding to the above constraints.

As a physical example, $\rho_F = 1.1$, $\rho_L = 1$, $\mu = 1$, $\sigma = 100$, $H = 1$, $h = 0.1$, $U_0 \sim 3$ (so that $\delta \sim 100$, $\Lambda \sim 1$, $T \sim 10$), all in CGS units, and (dimensionless) $\Omega \sim 0.1$ satisfy all the above constraints.

4. Numerical experiments

In order to study the effects of the oscillatory nonlinearity, (3.17) is solved numerically over extended spatial domains, $0 \leqslant x \leqslant L = 2\pi q$ where $q \gg 1$, subject to

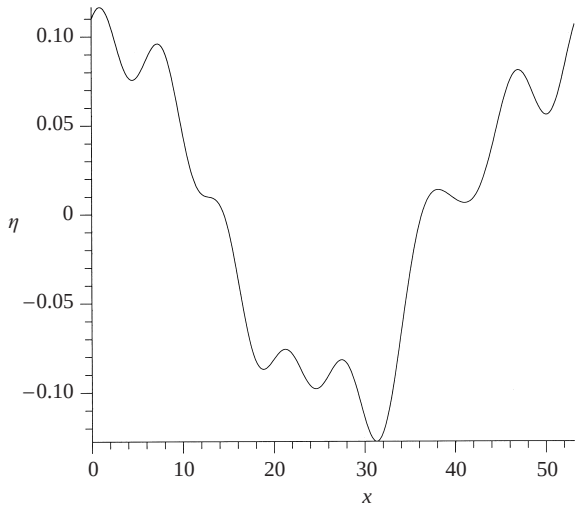

FIGURE 3. Initial disturbance, (4.1), used in the numerical simulations of the modified Kuramoto–Sivashinsky equation (3.17).

periodic boundary conditions. For large intervals, $q \gg 1$, we can expect that solutions with a characteristic lengthscale of $O(1)$ do not significantly depend on the specific type of boundary conditions except for small regions near the boundaries. (We have verified this fact using the method of lines scheme with non-periodic homogeneous boundary conditions.) A variation of a pseudospectral Fourier method is employed (see e.g. Frenkel & Indireshkumar 1996). Random initial conditions of the form

$$\eta\,(x,0) = A\cos qx + B\sum_{l=1}^{7}\cos\left((l+1)qx - \phi_l\right) \tag{4.1}$$

are used, where $B < A$ and ϕ_l is a randomly generated phase shift. An example of this initial condition is shown in figure 3.

4.1. *Low-frequency chaos*

The canonical KS equation exhibits deterministic chaos for sufficiently large intervals with periodic boundary conditions in certain parametric regions, and is recovered by setting $\Omega = 0$ in (3.17). (An extensive literature exists on the subject of numerical simulations of the KS equation. For smaller spatial intervals, the character of the solutions can vary with the interval length, quickly changing between chaotic and non-chaotic attractors. However, the solutions become predominantly chaotic when the length of the interval exceeds a certain critical value. See, e.g. Coward *et al.* (1995) and Wittenberg & Holmes (1999) and references therein, where the length value $L \approx 50$–60 is cited for the onset of the universal large-interval character of solutions. This value is close to those in the present work.) The interaction between the terms of the canonical KS equation has been thoroughly explained by Babchin *et al.* (1983) and Frenkel *et al.* (1987). Initially, a small-amplitude disturbance grows exponentially as a result of the destabilizing gravitational term (the second-order derivative in (3.17)), with a growth rate given by (3.18). Since the nonlinearity is proportional to η, at some point, it becomes as large as the linear terms, and prevents further growth.

A nonlinear hyperbolic wave equation is obtained if η is sufficiently large, so that the linear terms can be neglected. Since the wave speed is proportional to the amplitude of the disturbance, wave distortion and steepening occur. This steepening process is eventually slowed down and arrested by the surface tension. We observe similar phenomena in our numerical simulations of equation (3.17). Figure 4 shows snapshots of the interface at t=128.5, 160, 191.5 and 223, for $q = 6\sqrt{2}$, and $\Omega = 0.05$. Figures 4(a) and 4(c) correspond to times when $\cos \Omega t \approx \pm 1$. At low frequencies, there are sizable periods of time during the cycle when the amplitude of the nonlinear term is close to its maximum, and therefore we expect the system to behave like the canonical case, with the exception that the right-hand faces are steeper if the wave speed is positive and left-hand faces are steeper if the speed is negative. However, as $\cos \Omega t$ decreases, the effect of the nonlinearity weakens and eventually the destabilizing gravitational term gains control causing the amplitude of the disturbance to grow exponentially. Figures 4(b) and 4(d) correspond to cases when $\cos \Omega t \approx \mp 0.15$.

In figure 5, the modulus $\eta_m(t)$ of η, defined as

$$\eta_m(t) = \max_{0 \leqslant x \leqslant L} |\eta(x, t)|, \tag{4.2}$$

is plotted as a function of time using the same parameter values as in figure 4, and compared with the canonical KS equation. During periods of the cycle when the coefficient of the nonlinearity becomes small, η_m increases exponentially to a value close to 20. This is then followed by a rapid decrease to a value close to 2, which is close to the base value for the canonical KS equation. η_m does not deviate too much from this baseline value for a considerable part of the period, until the value of $\cos \Omega t$ is close to zero again, and the exponential growth cycle reappears. As Ω decreases, the maximum value of η_m increases since the amount of time during which the exponential growth can occur, increases. Note that $\Omega \to 0$ is a singular limit for equation (3.17). However, (3.17) is a good approximation only in a certain window of frequencies which is bounded away from zero (see § 3.2). This follows from the validity conditions given by the multiparameter perturbation approach. Otherwise, the large-time behaviour of the solutions of the oscillatory KS equation is statistically periodic. The variation of the mean of the peaks of η_m with respect to Ω was predicted semi-quantitatively by the quasi-equilibrium analysis of § 3.2.

The results of numerical experiments shown in figure 6 confirm the Ω^{-1} scaling of the amplitude predicted by the quasi-equilibrium theory in § 3.2, falling within the bounding lines given by the inequalities of (3.23). Here each estimate for η_{max} was obtained from the numerical simulations by taking the average of several of the large peaks of η_m. The experimental value of the coefficient C of the linear dependence $\eta_{max} = C\Omega^{-1}$ with the best fit to the numerical data is $C = 1.19$.

5. Transition to higher frequencies

As the frequency increases, η_{max} decreases. However, this behaviour holds only up to a certain point, Ω_c. For $\Omega > \Omega_c$, the system tends to solutions of a different type. The modified KS equation, (3.17), has the exact solutions

$$\eta(x, t) = \begin{cases} \dfrac{\Omega x}{\sin \Omega t + 1}, & 0 \leqslant x \leqslant X \quad \text{and} \quad L - X \leqslant x \leqslant L, \\ \dfrac{\Omega(x - \frac{1}{2}L)}{\sin \Omega t - 1}, & X \leqslant x \leqslant L - X, \end{cases} \tag{5.1}$$

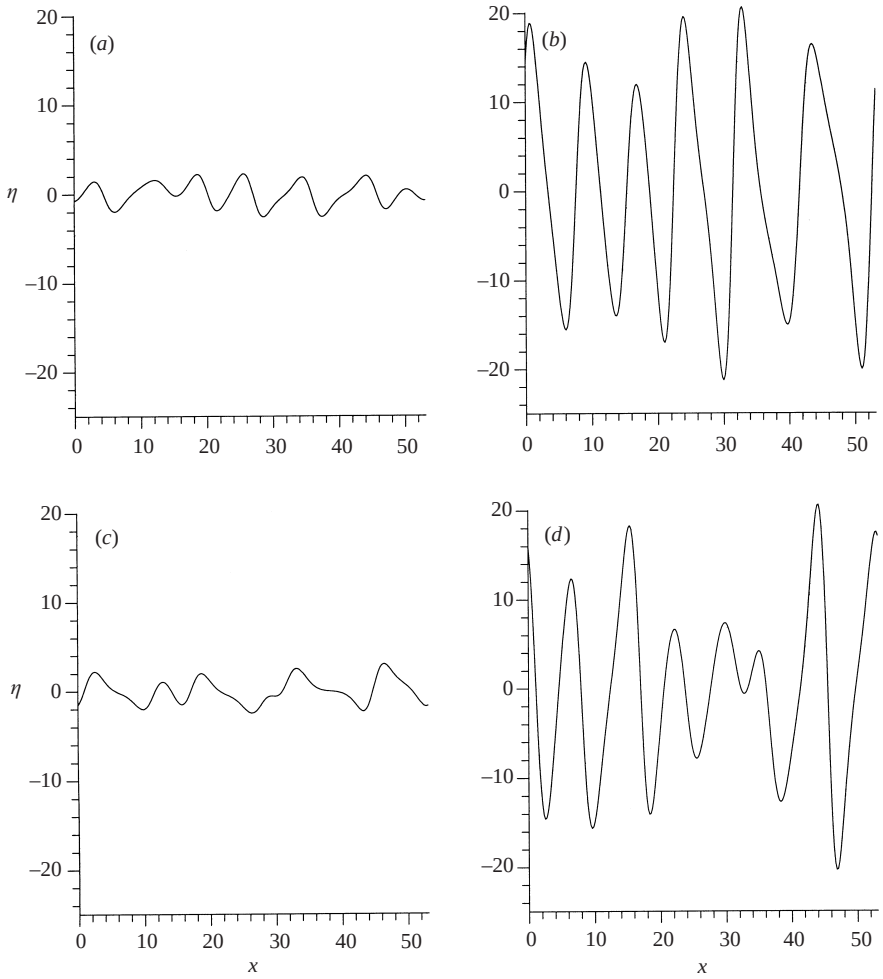

FIGURE 4. Instantaneous profiles of the time-asymptotic interface for a low frequency, $\Omega = 0.05$, for four instances of time separated by approximately a quarter of the period: (*a*) $t = 128.5$, (*b*) 160, (*c*) 191.5, (*d*) 223.

where $X = \frac{1}{4}L(\sin \Omega t + 1)$ and $\sin \Omega t \neq \pm 1$. This function is actually a solution to a wave equation consisting of the first two terms of (3.17), since the second and fourth derivatives of η with respect to x are obviously zero. It is continuous except when $\sin \Omega t = \pm 1$, but is not differentiable at $x = X$ and $x = L - X$. The discontinuity is smoothed out by the second and fourth derivative terms. Equation (5.1) can be thought of as an 'outer' solution that is approximately valid outside some time-dependent inner layer. We note that the canonical KS equation has an exact solution of a similar type, namely $\eta = x/t$. However, in contrast to (5.1), this solution decays with time.

From (5.1), $\eta_{\max} = \frac{1}{4}\Omega L$ by using the outer solution. Thus $\eta_{\max}$ grows with Ω, as opposed to low-frequency solutions where it decays as Ω^{-1}. An example of the time evolution for η at higher frequency is shown in figure 7, with $\Omega = 1$. The initial condition is the same as for the low-frequency cases, i.e. as given by (4.1). With time, the number of waves within the computational domain decreases, as the smaller-

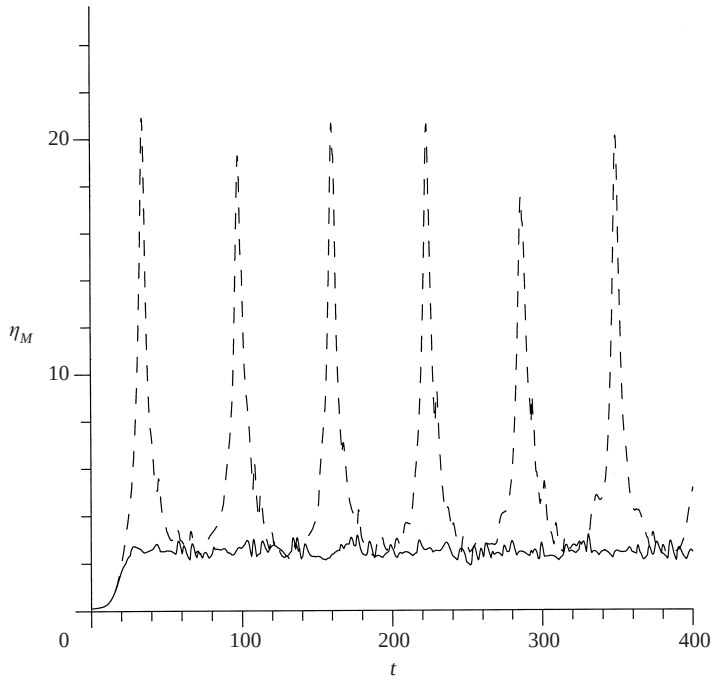

FIGURE 5. Time dependence of the maximum interface deflection: comparison between the canonical case, ———, $\Omega = 0$, and an oscillatory case, – – – –, $\Omega = 0.05$.

amplitude waves are absorbed by the larger and faster moving waves. Each time the wave absorption takes place, there is a sharp jump in η_m, as shown in figure 8, where η_m is plotted against time for various values of Ω. This absorption stops when the solution is close to (5.1), as shown in figure 9.

For Ω close to Ω_c, numerical solutions of (3.17) turn out to depend on the initial condition. If we start with the random condition given by (4.1), the large-time solution is similar to that observed above for very low frequencies. However, large-frequency behaviour is observed if (5.1) is used as an initial condition. This sensitivity to initial conditions can be seen from a plot of η_{max} versus time for Ω. If the initial condition is of the zigzag type as given by (5.1), the maximum amplitude decreases with frequency until $\Omega \approx 0.25$. Above this frequency, η_{max} increases almost linearly, and matches well with the maximum of (5.1) at large frequencies. If a random initial condition is used instead, the behaviour of η_{max} does not change for frequencies up to 0.25. However, η_{max} remains relatively flat for $0.25 < \Omega < 0.8$. At $\Omega \approx 0.8$, η_{max} increases sharply and attains the same value as in the case of the zigzag initial condition (see figure 10). Since, for the zigzag solution, the length of the computational domain is not much greater than the characteristic lengthscale, it is not *a priori* clear that the solution will remain essentially the same for the types of boundary conditions other than the periodic conditions we used. However, we have verified that this persistence of the zigzag solutions is the case, by using the numerical method of lines with non-periodic, homogeneous boundary conditions.

The parameter constraints obtained in § 3.2 for low-frequency solutions were based on the quasi-equilibrium theory which does not apply for the zigzag solutions. It is not difficult to modify the considerations of § 3.2 to obtain the parameter constraints appropriate here. One clear difference is that instead of $\Omega \ll 1$ we have now $\Omega \gtrsim 1$,

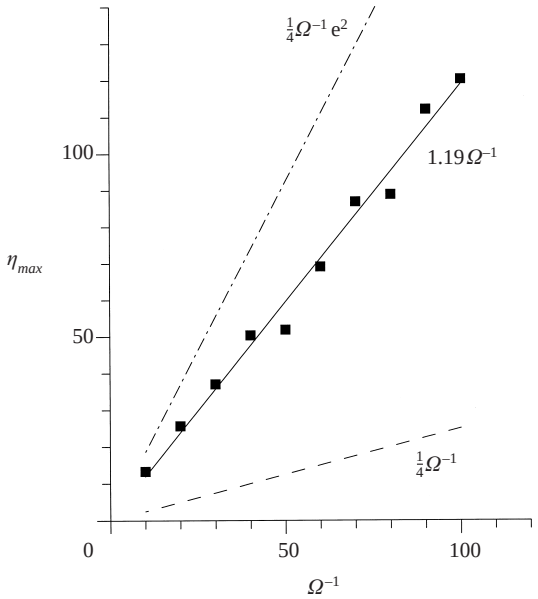

FIGURE 6. The linear dependence of the peak deflection of the interface on the reciprocal of the frequency: comparison between ■, numerical experiments, and – – –, —·—, the bounds given by the quasi-equilibrium theory. ———, least-squares fit to the experimental data.

i.e. (3.25) is replaced with

$$\Omega^* \gtrsim \frac{h^3\delta^2}{\mu\sigma}. \tag{5.2}$$

Also, we do not have now the condition (3.24) because the second derivatives of velocities corresponding to the zigzag solutions are exactly zero. Instead, we have the small-slope requirement $\eta^*/L^* \ll 1$, or $\eta_{max}A \ll \Lambda L$, (where from (5.1) $\eta_{max} \sim \Omega L$), or $\Omega^* \ll U_0/h$. Then, instead of (3.26), the small-amplitude requirement $\eta_{max}A \ll h$ becomes $\Omega^* \ll U_0/L^*$. This constraint can be combined with the previous one:

$$\Omega^* \ll \frac{U_0}{\max(h, L^*)}, \tag{5.3}$$

where L^* is the dimensional length of the domain. The constraint (3.27) remains unchanged. Instead of (3.28), we obtain

$$U_0 \ll \frac{L^*\nu}{h^2}. \tag{5.4}$$

Equation (3.30) is replaced with

$$\Omega^* \ll \frac{gL^*}{U_0 h}. \tag{5.5}$$

These constraints can be satisfied with the same values of parameters as those given at the end of § 3.2, except for the following changes: $U_0 \sim 10$, $\Omega^* \sim 1$, and $L^* \sim 1$.

However, the above considerations apply only to the outer solutions. Since the conditions of validity of the overall solution consisting of different outer regions connected by narrow boundary-layer regions are not known, the physical realizability of the zigzag solution remains a moot point.

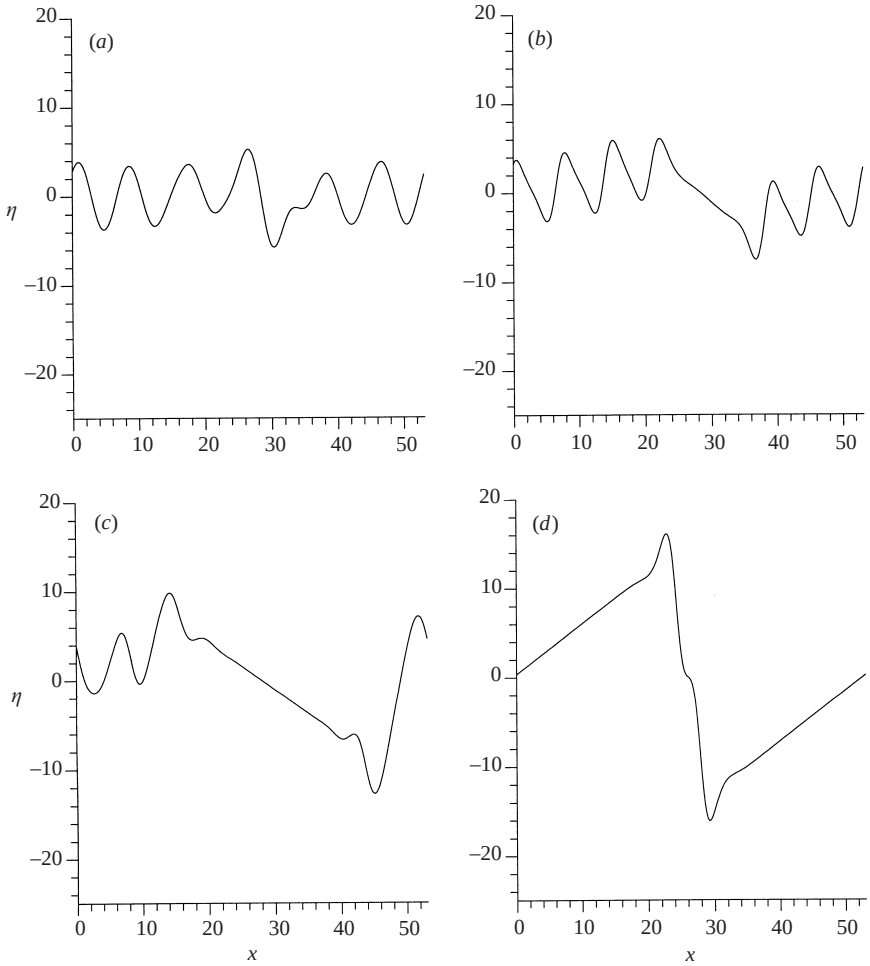

FIGURE 7. A series of snapshots of the interface for a higher frequency, $\Omega = 1$ at four instances of time, (*a*) $t = 40$, (*b*) 80, (*c*) 120, (*d*) 160, show the formation of a time-asymptotic profile.

6. Large-amplitude regimes and rupture of the film

Above, we have established, as our principal result, the existence of small-amplitude oscillatory regimes of film flow. Since the film thickness remains everywhere close to its average value, the possibility of rupture is clearly excluded. For other parametric regimes, such that the time-asymptotic disturbance of the film thickness is not small, the question of rupture is not that simple. The complete answer requires the numerical investigation of the 'large-amplitude' evolution equation replacing the 'small-amplitude' equation (3.17), as obtained by an appropriate rescaling of (3.11):

$$h_t + A(\cos \Omega t) h h_x + [h^3(h_x + h_{xxx})]_x = 0, \tag{6.1}$$

where we have, for simplicity, omitted the tildes.

Although such a complete numerical investigation, involving the space of the two parameters, the frequency and the amplitude, and, in addition, the dependence on initial conditions, is beyond the scope of the present paper, we include here some

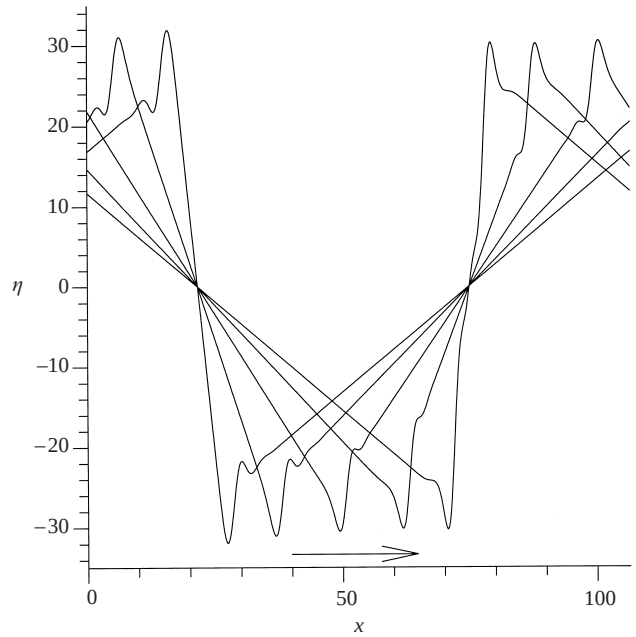

FIGURE 8. Large-time oscillation of the zigzag-like interface profile for frequency $\Omega = 1$.

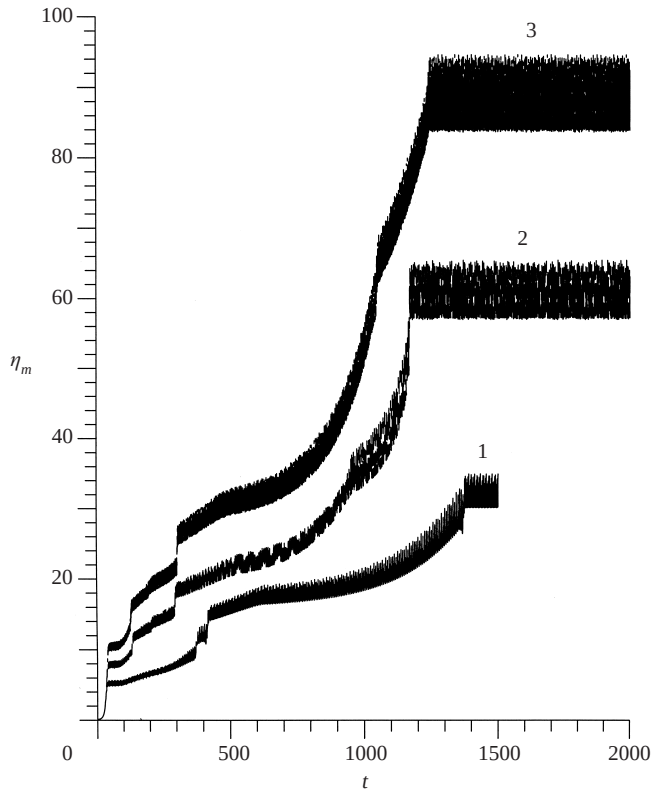

FIGURE 9. The maximum interface deflection η_m versus time, t, for $\Omega = 1$, 2 and 3. The jumps correspond to a decrease in the number of pulses.

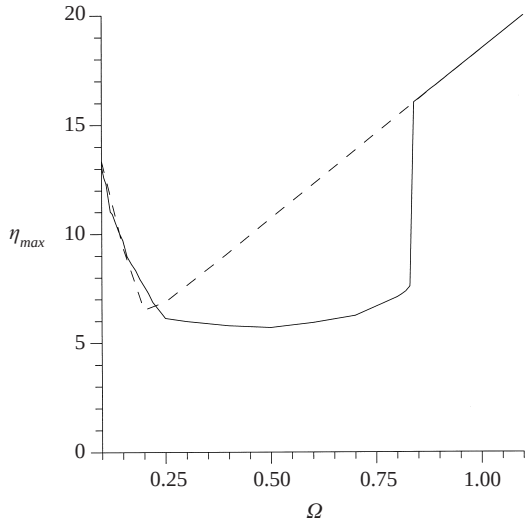

FIGURE 10. The effect of initial conditions on the maximum interfacial deflection as the frequency varies from small to large values. ———, random initial condition; – – – –, zigzag initial conditions.

preliminary results of numerical simulations of the highly nonlinear equation (6.1) bearing on the question of film rupture.

Equation (6.1) is readily rescaled to the form

$$h_t + (\cos \Omega t) h h_x + S[h^3(h_x + h_{xxx})]_x = 0, \tag{6.2}$$

where $S := 1/A$, which at $\Omega = 0$ reduces to the equation of a core–annular film flow studied in Frenkel & Kerchman (1994) (see also Kerchman & Frenkel 1994; Kerchman 1995; Frenkel & Indireshkumar 1996). Similar to these earlier studies, for large A, we can expect that the amplitude of the fluctuations is actually small (of order S), and the evolution is well approximated by the small-amplitude equation (3.17). Indeed, our simulations of the highly-nonlinear equation (6.1) with large A have essentially reproduced the small-amplitude results obtained above with the weakly-nonlinear equation (3.17). In particular, there is no rupture for $A \gg 1$.

In the opposite case, i.e. when A is not large, the weakly-nonlinear equation (3.17) is not good at all, and equation (6.1) should be used. Periodically, there occur time intervals during which the coefficient $A(\cos \Omega t)$ of the advective term nearly vanishes. As was first found by Hammond (1983), equation (6.1) with no advective term, $A = 0$, leads to rupture; at certain places along the film, the thickness approaches 0 as time tends to infinity. On the other hand, there are repeated time intervals with the coefficient $A(\cos \Omega t)$ being almost constant ($= A$), that is as if $\Omega = 0$. It was found in the aforementioned studies of such non-oscillatory (steady-flow) versions of equation (6.2), that the film thickness remains bounded away from zero (thus the film being prevented from rupture by the steady base flow, via the advective term of the equation). To decide between these contradictory indications as to the fate of the film, numerical simulations appear to be necessary. Such simulations with A of order one, starting with small-amplitude initial conditions, show that first, similar to the other highly-nonlinear equations, the film profile takes the form of a file of pulses whose amplitude is of order one, with a thinned film between them. When the frequency Ω is large, the time a pulse has to travel to one side is small, so the pulse

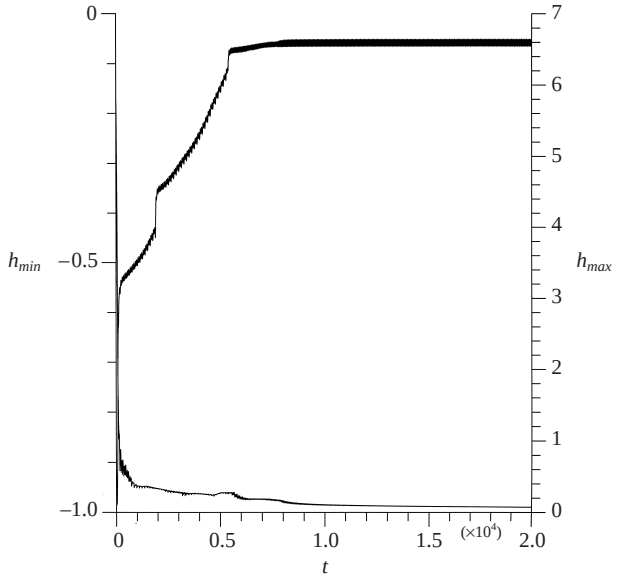

FIGURE 11. Minimum film thickness and maximum film thickness versus time for $\Omega = 0.05$ and $A = 0.25$.

essentially stays in the same place. Therefore, no collisions and coalescences of pulses (such as those in the steady-flow case of Kerchman & Frenkel 1994) occur, and the inter-pulse, 'substrate' film, as in the case of immobile pulses of the stagnant-film system (see Hammond 1983), continues indefinitely on its way to rupture. On the contrary, for smaller Ω, there are coalescences of pulses; they correspond to the fast increases of the maximum thickness in figure 11. In cases we observed, only one or two pulses (see figure 12 for the latter case) remained after the coalescence cascade which indicates that, depending on the initial conditions, more than one time-asymptotic configuration is possible. In figure 11 (see also figure 13), for $\Omega = 0.05$, there appears to be no end to the decrease in the minimum film thickness (which occurs in the substrate parts of the film), although some of our runs were as long as of order 10^5 time units. Figure 14 illustrates the drastic differences between this case and the steady-flow, no-rupture case: when the frequency in equation (6.1) is turned off, $\Omega = 0$, (at such t that $\cos \Omega t = 1$), the minimum thickness quickly returns to its (non-decreasing) steady-flow value (also shown is the fall of the minimum thickness if the whole advective term is turned off, by switching to $A = 0$, the case of no base flow). However, a small value of Ω does not necessarily imply rupture: when we switched to $\Omega = 0.001$ near the end of the run shown in figure 11 a new asymptotic regime developed (see figure 13) in which the minimum film thickness does not decay. In figure 13, in order to contrast the rupturing behaviour for $\Omega = 0.05$ and the non-rupturing one for $\Omega = 0.001$, the time interval between two neighbouring minimum film thickness data points is one period of oscillation, and each data point corresponds to the smallest film thickness during the time cycle. (For the two cases, the actual times corresponding to the zero point on the time axis in the figure are different – as, clearly, are the actual time intervals covered by the two data sets.) The notable difference between the two cases shown in figure 13 is as follows. For the case $\Omega = 0.05$, the lateral run length of the pulses is shorter than the computational

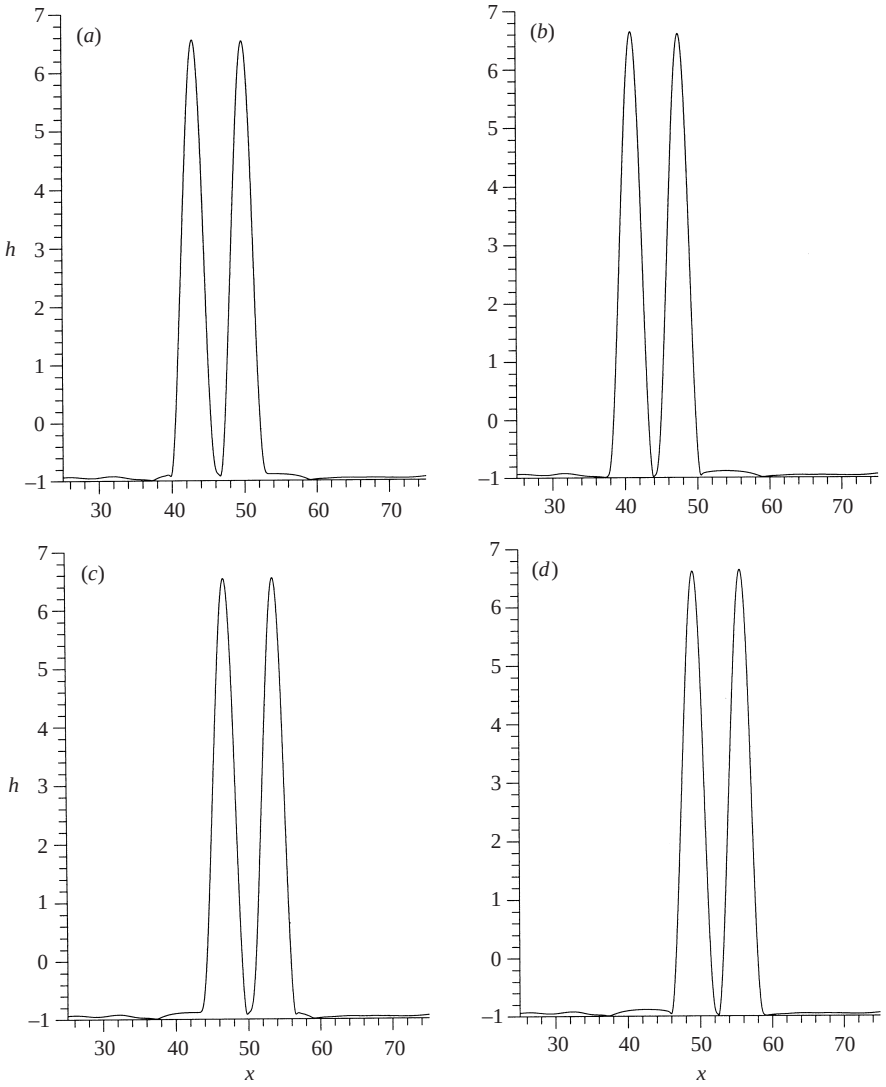

FIGURE 12. Instantaneous profiles of the time-asymptotic interface for a low frequency, $\Omega = 0.05$, for four instances of time separated by a quarter of the period: (*a*) $t = 19\,862.3$, (*b*) 19 893.7, (*c*) 19 925.1, (*d*) 19 956.5.

domain of periodicity (see figure 12; the smallest values of the minimum film thickness such as shown in figure 13 are observed to be reached at the instants when the pulses change their direction of motion, on the boundary between the pulses and the region never covered by the pulses during their motion.) In contrast, for the non-rupture case $\Omega = 0.001$, every point of the computational domain is reached by the (single, in this case) pulse. One possible conjecture would be that this difference is a decisive factor distinguishing between rupture and non-rupture. A follow-up conjecture is that for the infinite domain after the coalescences of pulses are completed, there are points between every two adjacent spatial intervals covered by neighbouring pulses where the rupture will develop. However, verifying these conjectures would require extensive computational work, and is a separate challenging project.

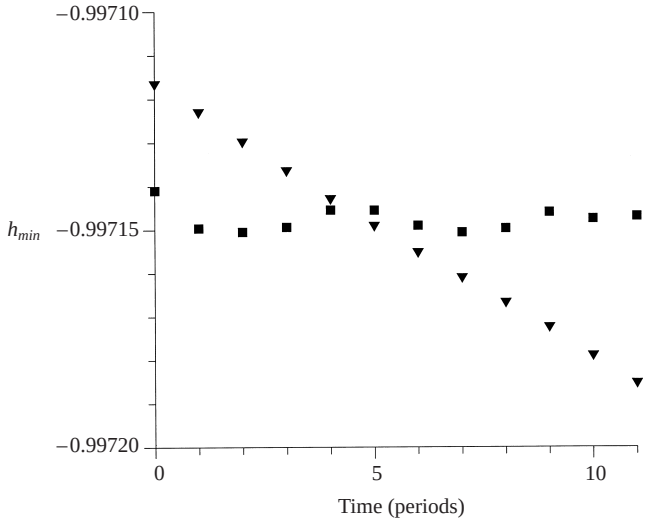

FIGURE 13. Minimum film-thickness data separated in time by the corresponding oscillation period showing ▼, film rupture for $\Omega = 0.05$ and ■, non-rupture for $\Omega = 0.001$, taken over eleven periods in each case.

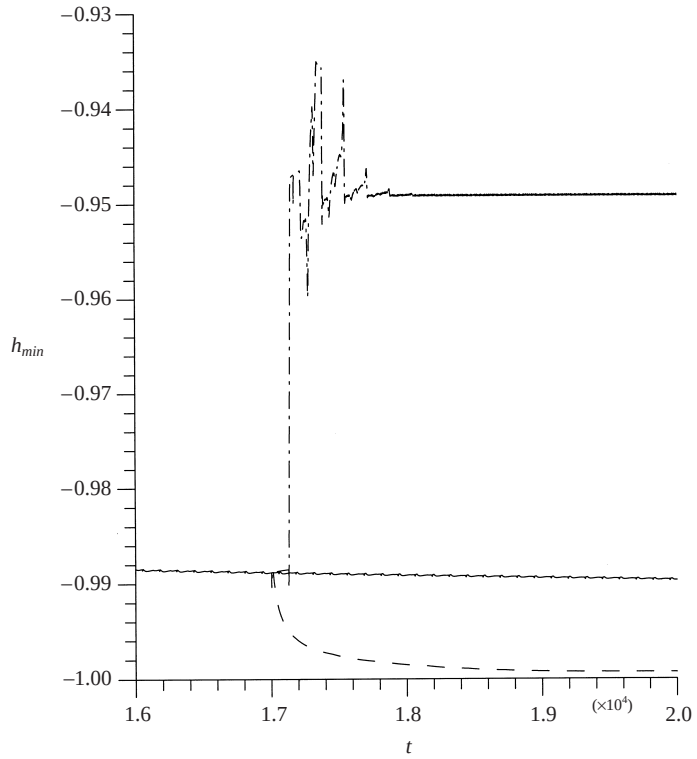

FIGURE 14. The minimum film thickness versus time for ———, steady flow ($A = 0.25$, $\Omega = 0$), —·—, oscillatory flow ($A = 0.25$, $\Omega = 0.05$) and – – – –, the static case ($A = 0$, $\Omega = 0$).

7. Discussion

We have shown that in certain parametric regimes, the nonlinear Rayleigh–Taylor instability of the oscillating Couette film flow is governed by a Kuramoto–Sivashinsky equation whose nonlinear term is modified by a time-oscillating factor (3.17). Our numerical simulations on extended spatial intervals demonstrate that there is nonlinear saturation of the Rayleigh–Taylor instability similar to the case of a steady primary flow (Babchin *et al.* 1983). Since the amplitude of the interface undulations is much smaller than the average film thickness, the Rayleigh–Taylor instability fails to rupture the film in these parametric regimes which imply certain windows of the velocity amplitude and frequency of the oscillations. This should be contrasted with pendant drops of Yiantsios & Higgins (1989), in which the film thickness between the drops is much smaller than the average thickness. For low frequencies, the large time behaviour of solutions shows periodic increases and decreases in the amplitude of the chaotic pulses of the usual Kuramoto–Sivashinsky type. The low-frequency scaling of the amplitude of the solutions on the frequency has been predicted by quasi-equilibrium theory, based on ideas stemming from those of Babchin *et al.* (1983). For high frequencies, simulations of the evolution equation uncover a completely different time-asymptotic behaviour, a piecewise-linear zigzag wave in an oscillatory motion. In a certain window of frequencies, the large-time behaviour of both types was observed at the same frequency depending on the initial conditions.

Our preliminary simulations of the large-amplitude regimes have shown both cases of non-rupture and rupture of the film at small frequencies, whereas the film always ruptures at larger frequencies. We have formulated certain conjectures from which it follows that a sufficiently extended film will always rupture. More exactly, it will reach such a small thickness that the long-range attractive van der Waals molecular forces become important. However, to verify whether this is the case will require further computational work.

For the future, it would be interesting to consider the Rayleigh–Taylor instability of the two-fluid film system for the case of multidirectional primary flows, taking into consideration the most general types of disturbances. (For some preliminary results, see Frenkel & Halpern (2000).)

Appendix. Long-wave analysis

In this Appendix, we give the exact equations of the problem and a further discussion of their relation to the simplified problem (3.1)–(3.6). We use a long-wave analysis similar to that of Yiantsios & Higgins (1989), but further complicated by the basic flow, which, moreover, is time-dependent.

The disturbances to the Nusselt type solutions (see § 2) for the flow in the film and the top liquid satisfy the following conservation of momentum and mass equations:

$$\rho_j\left(\frac{\partial u_j}{\partial t}+(U_j+u_j)\frac{\partial u_j}{\partial x}+v_j\left(\frac{\partial u_j}{\partial y}+\frac{\partial U_j}{\partial y}\right)\right)=-\frac{\partial p_j}{\partial x}+\mu_j\left(\frac{\partial^2 u_j}{\partial x^2}+\frac{\partial^2 u_j}{\partial y^2}\right), \quad \text{(A 1)}$$

$$\rho_j\left(\frac{\partial v_j}{\partial t}+(U_j+u_j)\frac{\partial v_j}{\partial x}+v_j\frac{\partial v_j}{\partial y}\right)=-\frac{\partial p_j}{\partial y}+\mu_j\left(\frac{\partial^2 v_j}{\partial x^2}+\frac{\partial^2 v_j}{\partial y^2}\right), \quad \text{(A 2)}$$

$$\frac{\partial u_j}{\partial x}+\frac{\partial v_j}{\partial y}=0, \quad \text{(A 3)}$$

where u_j and v_j are the disturbances of the horizontal and vertical velocity components, and p_j is the disturbance of the pressure. At the bottom and top plates, $y = -h$ and $y = H$, respectively, no-slip is required:

$$u_j = v_j = 0. \tag{A 4}$$

At the interface between the film and the top liquid, $y = \eta$, there is continuity of velocities, continuity of tangential stresses, and a jump in the normal stresses condition owing to surface tension, σ: $[\boldsymbol{u}_j] = 0$; $[\boldsymbol{\tau}_j \cdot \boldsymbol{t}] = 0$; and $[\boldsymbol{\tau}_j \cdot \boldsymbol{n}] = \kappa \boldsymbol{n}$ where $[\cdot]$ denotes the jump across the interface, $\boldsymbol{n}$ and $\boldsymbol{t}$ are the unit normal and tangent vectors to the interface, κ is the curvature of the interface, $\boldsymbol{\tau}_j = \boldsymbol{\sigma}_j \cdot \boldsymbol{n}$ is the stress vector and $\boldsymbol{\sigma}_j = -\boldsymbol{I} p_j + \mu_j(\nabla \boldsymbol{u}_j + \nabla \boldsymbol{u}_j^T)$ is the stress tensor. In component form these are as follows:

$$[u_j + U_j] = 0, \quad [v_j] = 0, \tag{A 5}$$

$$\left[(1 - \eta_x^2)\mu_j \left(\frac{\partial U_j}{\partial y} + \frac{\partial u_j}{\partial y} + \frac{\partial v_j}{\partial x}\right) - 4\mu_j \eta_x \frac{\partial u_j}{\partial x}\right] = 0, \tag{A 6}$$

$$\left[-p_j + 2\mu_j \frac{\eta_x^2 - 1}{\eta_x^2 + 1}\frac{\partial u_j}{\partial x} - 2\mu_j \frac{\eta_x}{\eta_x^2 + 1}\left(\frac{\partial U_j}{\partial y} + \frac{\partial u_j}{\partial y} + \frac{\partial v_j}{\partial x}\right)\right] = \sigma \frac{\eta_{xx}}{(\eta_x^2 + 1)^{3/2}} + g(\rho_L - \rho_F)\eta. \tag{A 7}$$

In addition, the position of the liquid-film interface, η, satisfies the kinematic boundary condition:

$$\frac{\partial \eta}{\partial t} + U_F \frac{\partial \eta}{\partial x} = -\frac{\partial Q}{\partial x}, \tag{A 8}$$

where Q is the disturbance of the streamwise flow rate, $Q = \int_{-h}^{\eta} u_f \, \mathrm{d}y$.

The above equations are non-dimensionalized using the same tentative scalings as in Yiantsios & Higgins (1989), and in addition appropriate scalings for the base velocities. The streamwise lengthscale Λ of the disturbances is assumed here to be long compared with the depth of the film, h, so that $\epsilon = h/\Lambda \ll 1$. When the film thickness is perturbed by an amount N, the destabilizing buoyancy term at the interface, δN (where $\delta = (\rho_L - \rho_F)g$) is counterbalanced by the capillary pressure term $\sigma N/\Lambda^2$ which 'tries' to restore the interface to its equilibrium position. Therefore, Λ is is of order $(\sigma/\delta)^{1/2}$. We scale the pressure on δN, x on Λ, and y on h. Assuming the Stokes flow limit, a horizontal velocity scale U_1 is obtained by balancing the disturbance pressure gradient in the horizontal direction and the dominant viscous term u_{yy}: $U_1 = \epsilon \delta h N/\mu_F$. This scale is not as obvious at it may seem; it involves an implicit assumption that the S terms in (3.7)–(3.8) are much smaller than the Π terms, which might not be the case for some parametric regimes. Continuity then provides the vertical velocity scale, $V_1 = \epsilon U_1$. The balance of the time derivative, η_t, and the vertical velocity term in the kinematic boundary condition gives the characteristic timescale, $T_1 = N/(\epsilon U_1)$. The velocity of the base flow in the film is scaled on U_0 so that the scale of the velocity shear rate $\partial U_F/\partial y$ is U_0/h (see (2.3)) provided there is no intrinsic lengthscale of U_F shorter than h. For the oscillatory basic flow, (2.2), this implies the condition

$$|k_F h| \ll 1. \tag{A 9}$$

The dimensionless momentum and continuity equations in the film region are:

$$\frac{\epsilon^2\rho_F\delta h^3}{\mu_F^2}\left(\frac{\partial u_F}{\partial t}+\alpha\left(u_F\frac{\partial u_F}{\partial x}+v_F\frac{\partial u_F}{\partial y}\right)\right)+\frac{\epsilon\rho_F U_0 h}{\mu_F}\left(U_F\frac{\partial u_F}{\partial x}+v_F\frac{\partial U_F}{\partial y}\right)$$
$$=-\frac{\partial p_F}{\partial x}+\epsilon^2\frac{\partial^2 u_F}{\partial x^2}+\frac{\partial^2 u_F}{\partial y^2}, \quad \text{(A 10)}$$

$$\frac{\epsilon^4\rho_F\delta h^3}{\mu_F^2}\left(\frac{\partial v_F}{\partial t}+\alpha\left(u_F\frac{\partial v_F}{\partial x}+v_F\frac{\partial v_F}{\partial y}\right)\right)+\frac{\epsilon^3\rho_F U_0 h}{\mu_F}U_F\frac{\partial v_F}{\partial x}$$
$$=-\frac{\partial p_F}{\partial y}+\epsilon^2\left(\epsilon^2\frac{\partial^2 v_F}{\partial x^2}+\frac{\partial^2 v_F}{\partial y^2}\right), \quad \text{(A 11)}$$

$$\frac{\partial u_F}{\partial x}+\frac{\partial v_F}{\partial y}=0, \quad \text{(A 12)}$$

where the condition

$$\alpha=N/h<1 \quad \text{(A 13)}$$

is assumed.

In the top liquid, assuming that $H>\Lambda$, the vertical coordinate is scaled on Λ the same as the horizontal coordinate, the velocity disturbances are scaled on U_1, the pressure on $\mu_L U_1/\Lambda$, and the basic velocity on $\Lambda U_0/h$ (where for simplicity we assume that H is not much greater than Λ, $H\sim\Lambda$), so that the momentum and continuity equations are:

$$\frac{\rho_L\delta h^3}{\mu_L\mu_F}\left(\frac{\partial u_L}{\partial t}+\alpha\left(u_L\frac{\partial u_L}{\partial x}+v_L\frac{\partial u_L}{\partial Y}\right)\right)+\frac{\rho_L U_0\Lambda^2}{\mu_L h}\left(U_L\frac{\partial u_L}{\partial x}+v_L\frac{\partial U_L}{\partial Y}\right)$$
$$=-\frac{\partial p_L}{\partial x}+\frac{\partial^2 u_L}{\partial x^2}+\frac{\partial^2 u_L}{\partial Y^2}, \quad \text{(A 14)}$$

$$\frac{\rho_L\delta h^3}{\mu_L\mu_F}\left(\frac{\partial v_L}{\partial t}+\alpha\left(u_L\frac{\partial v_L}{\partial x}+v_L\frac{\partial v_L}{\partial Y}\right)\right)+\frac{\rho_L U_0\Lambda^2}{\mu_L h}U_L\frac{\partial v_L}{\partial x}$$
$$=-\frac{\partial p_L}{\partial Y}+\frac{\partial^2 v_L}{\partial x^2}+\frac{\partial v_L}{\partial Y^2}, \quad \text{(A 15)}$$

$$\frac{\partial u_L}{\partial x}+\frac{\partial v_L}{\partial Y}=0. \quad \text{(A 16)}$$

The dimensionless conditions of continuity of interfacial velocities are

$$u_L=u_F+\Delta\left(U_F-\frac{\Lambda}{h}U_L\right), \quad v_L=v_F, \quad \text{(A 17)}$$

where $\Delta=U_0/U_1$.

Our scaling presupposes that if u_F and u_L are of order of magnitude one, then the combination in parentheses in (A 17) must be of order of magnitude one or less. It can be shown that this requirement on the basic velocities is satisfied in the case of $m=O(1)$ and small-amplitude regimes as a consequence of the S terms in (3.7)–(3.8) being small. In other parametric regimes, the scale of u_L might be greater than that of u_F, being determined by the basic velocity terms in (A 17).

The tangential stress condition becomes

$$-4\alpha\epsilon^2\frac{\partial u_F}{\partial x}\eta_x + \left(1-\alpha^2\epsilon^2\eta_x^2\right)\left(\Delta\frac{\partial U_F}{\partial y}+\frac{\partial u_F}{\partial y}+\epsilon^2\frac{\partial v_F}{\partial x}\right)$$
$$= -4\alpha\epsilon^2 m\frac{\partial u_L}{\partial x}\eta_x + m\left(1-\alpha^2\epsilon^2\eta_x^2\right)\left(\Delta\frac{\partial U_L}{\partial Y}+\epsilon\frac{\partial u_L}{\partial Y}+\epsilon\frac{\partial v_L}{\partial x}\right). \quad \text{(A 18)}$$

The normal stress condition (A 7) can be simplified by substituting the sum of the terms in parentheses, as found from the tangential condition (A 6). This yields

$$-(p_F - m\epsilon^2 p_L) - 2\epsilon^2\frac{1+\alpha^2\epsilon^2\eta_x^2}{1-\alpha^2\epsilon^2\eta_x^2}\left(\frac{\partial u_F}{\partial x}-m\frac{\partial u_L}{\partial x}\right) = \frac{\eta_{xx}}{(1+\alpha^2\epsilon^2\eta_x^2)^{3/2}}+\eta. \quad \text{(A 19)}$$

Since in the dimensionless equations all the variable quantities are scaled to be of order of magnitude one and taking into account $\epsilon \ll 1$, we can omit all expressions multiplied by positive powers of ϵ, so that for the film the long-wave Stokes flow equations (3.1)–(3.6) are obtained. However, this is legitimate only if a number of additional requirements are satisfied. Namely, the ratio of the time-dependent to viscous terms must be small, $\epsilon^2\rho_F\delta h^3/\mu_F^2 \ll 1$, and the Reynolds number must also be small,

$$\frac{\epsilon\rho_F U_0 h}{\mu_F} \ll 1. \quad \text{(A 20)}$$

Also, for the top-liquid terms in the normal stress condition to be negligible, it is only required that $\epsilon m \ll 1$; for simplicity we assume $m \sim 1$ (and $\rho_L/\rho_F \sim 1$). (If $\epsilon m \ll 1$ is not the case, it is still possible to obtain an evolution equation. It will contain non-local integral terms leading to dispersive effects, similar to Frenkel (1988) and Papageorgiou *et al.* 1990.)

Similar to Yiantsios & Higgins (1989), it is not necessary to have Stokes flow in the top liquid. If the inertial terms are important, there is a viscous boundary layer near the interface. A new effective scale for disturbances appears which should be much larger than h for the viscous top-liquid terms to be negligible in the boundary conditions. Estimating the lengthscale from the balance of the viscous terms and the term containing $U_L(\partial u_L/\partial x)$ in the momentum equation (A 14) we arrive at the condition $(\epsilon\rho_F U_0 h/\mu_F)^{1/3} \ll 1$, just slightly stronger than the condition of smallness of the Reynolds number given above (cf. (A 20)).

Most of the above conditions expressed by inequalities contain the basic parameters only. However, for example, the condition (A 13) contains the amplitude N which is originally not in terms of the basic parameters. The maximum η oscillates with time, and the dependence of N on the parameters can only be obtained by the analysis of the evolution equation as carried out in § 3.1. Such considerations as used in this Appendix should be regarded as heuristic arguments only which can suggest the form of the simplified problem. However, we must be cautious as regards the validity domain of the evolution equation; in the end, we should verify that all the scales assumed in non-dimensionalization are reproduced as a result of the solution of the simplified problem and the evolution equation.

If the wave amplitude N is to be small, the above inequality constraints are the consistency conditions of § 3.2.

REFERENCES

Babchin, A. J., Frenkel, A. L., Levich, B. G. & Sivashinsky, G. I. 1983 Nonlinear saturation of Rayleigh–Taylor instability in thin films. *Phys. Fluids* **26**, 3159–3161.

Berenson, J. 1962 Experiments on pool boiling heat transfer. *Intl J. Heat Mass Transfer* **5**, 985–999.

Berning, M. & Rubenchik, A. M. 1998 A weakly nonlinear theory for the dynamical Rayleigh–Taylor instability. *Phys. Fluids* **7**, 1564–1587.

Canright, D. & Morris, S. 1993 Buoyant instability of a viscous film over a passsive fluid. *J. Fluid Mech.* **255**, 349–372.

Chandrasekhar, S. 1961 *Hydrodynamics and Hydromagnetic Stability*. Oxford University Press.

Coward, A. V. & Papageorgiou, D. T. 1994 Stability of oscillatory two-phase Couette flow. *IMA J. Appl. Maths* **55**, 75–93.

Coward, A. V., Papageorgiou, D. T. & Smyrlis, Y. S. 1995 Nonlinear stability of oscillatory core–annular flow: a generalized Kuramoto–Sivashinsky equation with time period coefficients. *Z. angew Math. Phys.* **46**, 1–39.

Coward, A. V. & Renardy, Y. Y. 1997 Small-amplitude oscillatory forcing on two-layer plane channel flow. *J. Fluid Mech.* **334**, 87–109.

Davis, S. H. 1976 The stability of time-periodic flows. *Ann. Rev. Fluid Mech.* **8**, 57–74.

Fermigier, M., Limat, L., Wesfreid, J. E., Boudineux, P. & Quillet, C. 1992 Two-dimensional patterns in Rayleigh–Taylor instability of a thin layer. *J. Fluid Mech.* **236**, 349–383.

Frenkel, A. L. 1988 Nonlinear saturation of core–annular flow instabilities. In *Proc. Sixth Symp. on Energy Engineering Sciences*, pp. 100–107. US Dept of Energy, Argonne, IL.

Frenkel, A. L., Babchin, A. J., Levich, B. G., Shlang, T. & Sivashinsky, G. I. 1987 Annular flow can keep unstable flow from breakup: nonlinear saturation of capillary instability. *J. Colloid Interface Sci.* **115**, 225–233.

Frenkel, A. L. & Halpern, D. 2000 On saturation of Rayleigh–Taylor instability. In *IUTAM Symp. on Nonlinear Waves in Multiphase Flow* (ed. H. Chang), pp. 69–79. Kluwer.

Frenkel, A. L. & Indireshkumar, K. 1996 Derivation and simulations of evolution equations of wavy film flows. In *Math Modeling and Simulation in Hydrodynamic Stability* (ed. D. N. Riahi), pp. 35–81. World Scientific, Singapore.

Frenkel, A. L. & Indireshkumar, K. 1999 Wavy film flows down an inclined plane: perturbation theory and general evolution equation for the film thickness. *Phys. Rev.* E **60**, 4143–4157.

Frenkel, A. L. & Kerchman, V. I. 1994 On large amplitude waves in core–annular flows. In *Proc. 14th IMACS Congress on Computations and Applied Mathematics* (ed. W. F. Ames), pp. 397–400. Atlanta, GA.

Hall, P. 1975 The stability of Poiseuille flow modulated at high frequencies. *Proc. R. Soc. Lond.* A **344**, 453–464.

Halpern, D. & Grotberg, J. B. 1992 Fluid-elastic instabilities of liquid lined flexible tubes: airway closure, *J. Fluid Mech.* **244**, 615–632.

Halpern, D., Moriarty, J. A. & Grotberg, J. B. 1999 Capillary-elastic instabilities with an oscillatory forcing function. In *IUTAM Symp. on Non-linear Singularities in Deformation and Flow* (ed. D. Durban & J. R. A. Pearson), pp. 243–255. Kluwer.

Hammond, P. 1983 Nonlinear adjustment of a thin annular film of viscous fluid surrounding a thread of another within a circular pipe. *J. Fluid Mech.* **137**, 363–384.

Johnson, M., Kamm, R. D., Ho, L. W., Shapiro, A. & Pedley, T. J. 1991 The nonlinear growth of surface-tension driven instabilities of a thin annular film. *J. Fluid Mech.* **233**, 141–156.

Joseph, D. D. & Renardy, Y. 1991 *Fundamentals of Two-Fluid Dynamics, vol. I: Mathematical Theory and Applications; vol. II. Lubricated Transport, Drops, and Miscible Liquids*. Springer.

Kerchman, V. 1995 Strongly nonlinear interfacial dynamics in core–annular flows. *J. Fluid Mech.* **290**, 131–166.

Kerchman, V. I. & Frenkel, A. L. 1994 Interactions of coherent structures in a film flow – simulations of a highly nonlinear evolution equation. *Theor. Comput. Fluid Dyn.* **6**, 235–254.

von Kerczek, C. H. 1982 Instability of oscillatory plane Poiseuille flow. *J. Fluid Mech.* **116**, 91–114.

von Kerczek, C. H. 1987 Stability characteristics of some oscillatory flows – Poiseuille, Eckman and films. In *Stability of Time Dependent and Spatially Varying Flows* (ed. D. Dwoyer & M. Hussaini). Springer.

Kilkenny, J. D., Glendinning, S. G., Haan, S. W., Hammel, B. A., Lindl, J. D., Munro, D., Remington, B. A., Weber, S. V., Knauer, J. P. & Verdon, C. P. 1994 A review of the ablative stabilization of the Rayleigh–Taylor instability in regimes relevant to inertial confinement fusion. *Phys. Plasmas* **1**, 1379–1388.

King, M. R., Leighton, D. T. & McCready, M. J. 1999 Stability of oscillatory two-phase Couette flow: theory and experiment. *Phys. Fluids* **11**, 833–844.

Or, A. C. 1998 Finite-wavelength instability in a horizontal liquid layer on an oscillating plane. *J. Fluid Mech.* **335**, 213–232.

Papageorgiou, D., Maldarelli, C. & Rumschitzki, D. 1990 Nonlinear interfacial stability of core annular film flows. *Phys. Fluids* A **2**, 268–271.

Rayleigh, Lord 1883 Investigation of the character of the equilibrium of an incompressible heavy fluid of variable density. *Proc. Lond. Math. Soc.* **14**, 170–197.

Ribe, N. M. 1998 Spouting and planform selection in the Rayleigh–Taylor instability of miscible viscous fluids. *J. Fluid Mech.* **377**, 27–45.

Taylor, G. I. 1950 The instability of liquid surfaces when accelerated in a direction perpendicular to their planes. *Proc. Roy. Soc.* A **201**, 192–196.

Tryggvason, G. & Unverdi, S. O. 1990 Computations of three-dimensional Rayleigh–Taylor instability. *Phys. Fluids* A **2**, 656–659.

Whitehead, J. A. 1988 Fluid models of geological hotspots. *Ann. Rev. Fluid Mech.* **20**, 61–87.

Wittenberg, R. & Holmes, P. 1999 Scale and space localization in the Kuramoto–Sivashinky equation. *Chaos* **9**, 452–465.

Yiantsios, G. & Higgins, G. 1989 Rayleigh–Taylor instability in thin viscous films. *Phys. Fluids* A **1**, 1484–1501.

Yih, C. S. 1967 Instability due to viscosity stratification. *J. Fluid Mech.* **27**, 337–352.

Yih, C. S. 1968 Instability of unsteady flows or configurations. Part 1. Instability of a horizontal liquid layer on an oscillating plate. *J. Fluid Mech.* **31**, 737–751.